*Invited Paper*

# High-Power THz-Waves using gyrotrons: new physics results

Stefano Alberti [*], Falk Braunmueller, Trach Minh Tran, Jean-Philippe Hogge, Jérémy Genoud, and Minh Quang Tran
Centre de Recherches en Physique des Plasmas (CRPP),
Ecole Polytechnique Fédérale de Lausanne (EPFL), Station 13, 1015 Lausanne, Switzerland
[*] Email: stefano.alberti@epfl.ch

(Received December19, 2013)

**Abstract**: Gyrotrons are high-power coherent radiation sources based on the cyclotron maser instability. Since more than three decades the research and development of gyrotrons has been essentially driven from the need of high-power MW-level sources in the THz frequency range (0.1-1 *THz*) for electron cyclotron resonance heating of magnetically confined plasmas such as in ITER and DEMO. A more recent spin-off research activity has led to the development of lower power (1-100 *W*) gyrotrons with frequencies belonging to the THz domain. One of the main applications in the THz domain is in the field of Dynamic Nuclear Polarization Nuclear Magnetic Resonance spectroscopy (DNP/NMR).

With a THz gyrotron oscillator developped for DNP/NMR spectroscopy and operating at 260 *GHz*, novel operational regimes have been recently experimentally demonstrated in which the non-linear interaction excites a finite number of side-bands and eventually ends in a chaotic dynamics of the THz radiation field. The route to chaos via a period doubling cascade dynamics is experimentally observed and is supported by numerical simulations. In presence of phase-locked frequency-equidistant side-bands, a novel regime characterized by high-power nanosecond pulses is experimentally observed and is associated to a self-consistent Q-switch mechanism in which the cavity diffraction quality factor dynamically varies by nearly two orders of magnitude on a subnanosecond timescale. This novel regime is also well predicted with the self-consistent TWANG code and may open up new applications for gyrotrons.

**Keywords**: Terahertz Waves, Gyrotron Oscillator, Non-stationary regime (automodulation), Chaos, Nanosecond pulses, mode-locking, Q-switch.

**doi:** 10.11906/TST.023-038.2014.03.03

## 1. Introduction

Dynamic Nuclear Polarization for Nuclear Magnetic Resonance spectroscopy (DNP/NMR) is a fast evolving domain which has benefited from continuing development of THz instrumentation [1-5]. This research activity stems from the research and development of high-power THz-wave gyrotrons [6-9] for heating of magnetically confined plasmas [10] and encompasses fields ranging from the development of coherent high-power THz radiation sources (typically gyrotrons), development of quasi-optical techniques for controlling the wave polarization and efficiently transmitting the radiation to the sample, and, finally, optimizing the coupling of the THz radiation to the electron spins in the sample under study [4, 5]. In this paper we report on experimental and numerical results obtained with a frequency-tunable gyrotron operating at

260.5 *GHz* developed for DNP/NMR spectroscopy. With this gyrotron, in addition to the usual operation on a stationary regime characterized by a single frequency for a given transverse mode, $TE_{7,2}$, new physics results have been obtained in non-stationary regimes characterized by the excitation of frequency equidistant side-bands [11, 12]. Figure 1 summarizes and illustrates the domains of operation for stationary and non-stationary regimes in the parameter space defined by the cavity magnetic field, B, and the electron beam-current, $I_b$. In this same figure, the top and right axis represent the normalized detuning and normalized currents, respectively [11, 13]. It has to be noticed, that for positive normalized detuning, Δ, the gyrotron is operated in the so called gyro-traveling-wave (gyro-TWT) regime, whereas for negative Δ's a gyro-backward-wave regime (gyro-BWO) is enforced, the latter being dominated by self-consistent effects. The non-stationary regimes have been extensively studied experimentally [11, 12] and are also supported by numerical simulations using the time-dependent self-consistent mono-mode code TWANG developed at CRPP [14].

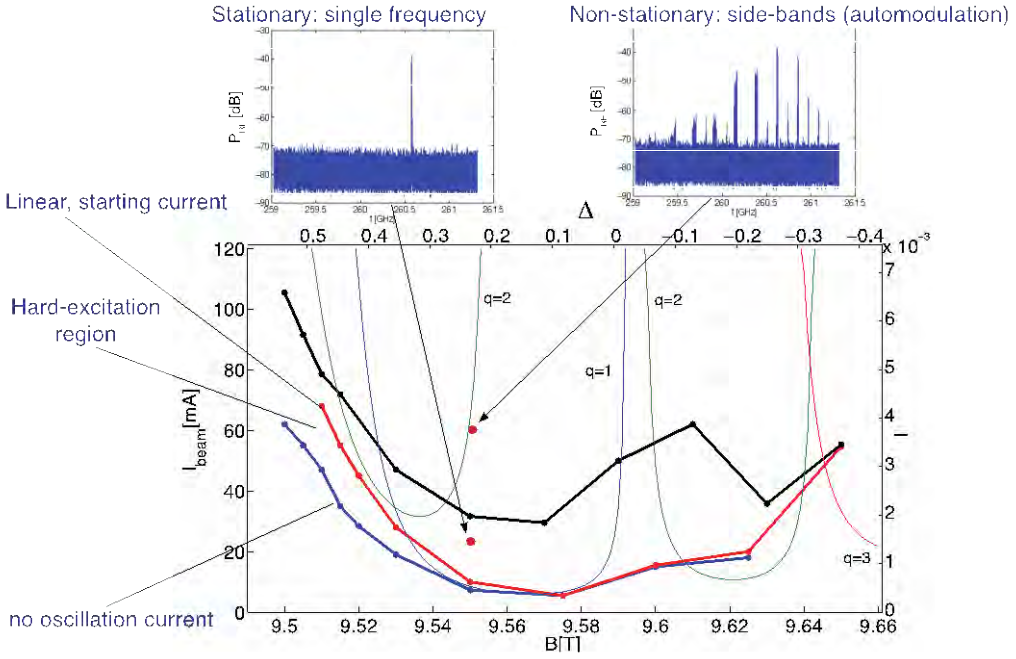


Fig. 1 Experimentally observed operating regimes in the $B_0$-$I_b$ plane for the $TE_{7,2}$ transverse mode. All the experimental points are represented by filled circles connected by a line. The red line represents the starting current curve. The blue line, the no-oscillation region. The black line the starting current curve for nonstationary operating points characterized by the sudden appearance of side-bands [11]. The thin continuous lines are the calculated starting current curves for the q=1–3 longitudinal modes of the $TE_{7,2}$ transverse mode and based on a cold cavity profile. The beam parameters for this calculation are: accelerating voltage,$V_b$ = 15.5 *kV*, electron beam radius, $r_b$ = 1.36 *mm*, pitch angle, α = 1.7. Other relevant parameters are given further in this paper and/or in [11]. For a magnetic field $B_0$=9.55 *T*, two operating points, one for a stationary regime and the other for a non-stationary regime are indicated by the large red filled circle with the corresponding spectra shown in the insets.

In this paper we will concentrate on two specific operation points, defined later on in the paper, for non-stationary regimes in which, first, the route to chaos via period doubling cascade has

been experimentally observed, and, second, a nanosecond pulsed regime has been found and is interpreted as the consequence of a self-consistent Q-switch (SQS) effect in which the diffraction quality factor is dynamically modulated via the nonlinear interaction of different mode locked side bands. Non-stationary regimes in gyrotron oscillators have been studied essentially theoretically in the past [15, 16, 13] as well as experimentally [17] and we will discuss in detail how these new results compare with the ones presented in these past articles.

The paper is organized as follows: Section 2 is devoted to the general design characteristics of the gyrotron together with the experimental setup and diagnostics used. In Section 3, the gyrotron results for an operation on a stationary regime will be given with a particular emphasis on the first application for DNP/NMR experiments to be carried out at EPFL.

Section 4 discusses the novel results on non-stationary operating points concentrating on the two specific operational points mentioned above: route to chaos and SQS. Section 5 will discuss the results in the frame of the existing models and draw the conclusion.

## 2. Design characteristics of frequency-tunable gyrotron oscillator for DNP/NMR spectroscopy, modeling tools and fast spectroscopy diagnostics.

The modular 260.5 *GHz* frequency-tunable gyrotron (>1 *GHz* bandwidth) with power in excess of 100 *W* has been designed at CRPP whereas the fabrication of the first modular prototype was carried out by the industrial partner Thales Electron Devices. Details of the design features can be found in reference [11] and a schematic of the essential gyrotron setup is shown in Fig. 2.

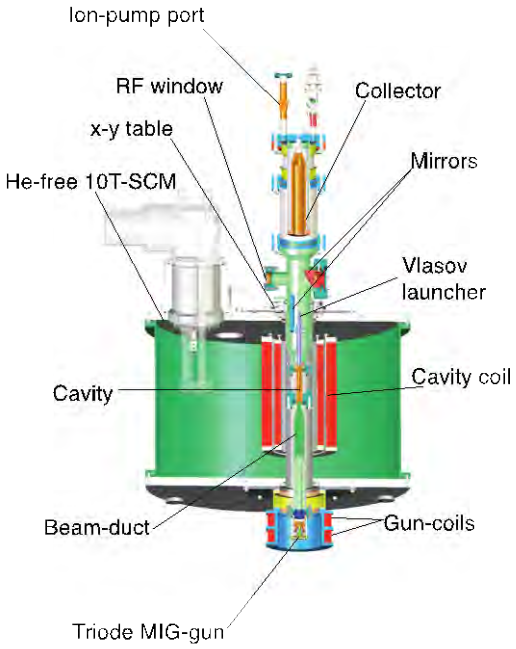


Fig. 2 Schematic of the gyrotron main components.

The main experimental control parameters are: a) cavity magnetic field amplitude, b) gun-coils magnetic field amplitude and gradient, c) beam energy via the main power supply, d) pitch-angle via the mode-anode power supply, e) the beam current via the cathode heating power supply. The pitch-angle as well as the beam velocity spread can be moderately controlled via the gun-coils and the beam current also depends on the anode voltage via the Schottky effect. The entire gyrotron can be moved using an optical precision x-y table for aligning the gyrotron mechanical axis with respect to the magnetic field axis. The collector is insulated which gives the possibility to experimentally verify that full electron beam transmission is obtained from cathode to collector. Other details are to be found in reference [11].

The interaction space parameters are summarized in Fig. 3, where the different profiles along the gyrotron axis are shown: cavity magnetic field profile (in green), cavity-launcher radius (in blue), electron beam radius (in yellow) and beam parameters. Also shown in red is the non-selfconsistent (cold-cavity) calculated amplitude of the rf-electric field profile for the fundamental longitudinal mode (q=1), $TE_{7,2,1}$.

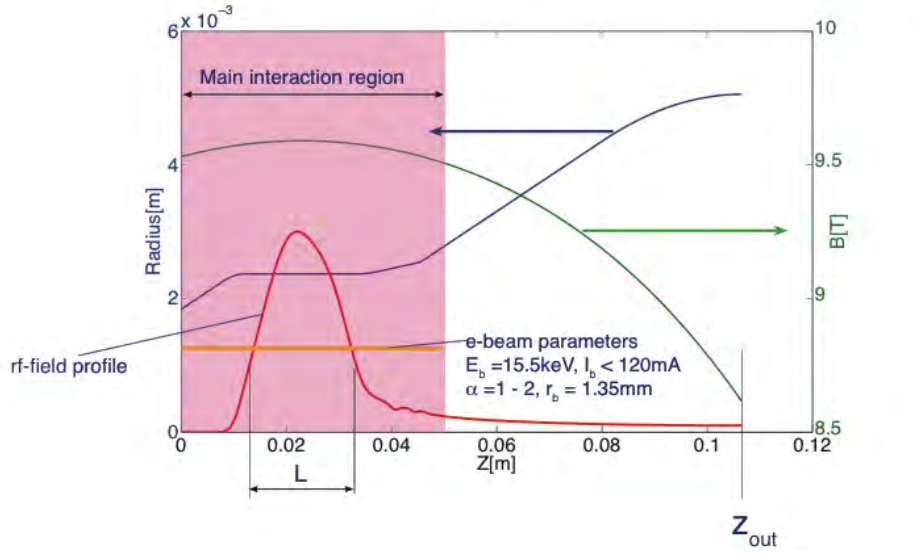


Fig. 3 Description of the interaction space parameters as used in the simulation with the TWANG code.

The same interaction space, as shown in Fig.3, is considered for the modeling with the monomode code TWANG. It is important to mention that the relatively low order mode for the chosen TE cavity mode, $TE_{7,2}$, makes that the entire complex dynamics presented in this paper is fully given by the longitudinal self-consistent rf-field profile and not by mode competition with other transverse modes as it is the case for high-power gyrotrons for fusion applications. The numerical approach in TWANG is extensively described in [14], and we emphasize the fact that the model is based on the commonly adopted assumption that the electron time of flight in the interaction region, $\tau_b$, is significantly shorter than the time scale of the rf-field envelope variation [18]. We will come back to the limitations associated to this assumption in the last section of the paper. Another point to be highlighted is that in TWANG, at the interaction space exit, $z=z_{out}$, a

radiation boundary condition is implemented which insures that full-transmission (i.e. no reflection) of the rf-wave is obtained at the exit of the interaction space.

The key diagnostics for characterizing the complex dynamics described in this paper are shown in Fig. 4. The particular feature of this setup, is that with the data acquired with the fast oscilloscope one can perform fast spectroscopy (FFT) with a time resolution of typically 100 *ns* which is nearly two orders of magnitude better than the time resolution of the spectrum analyser. As will be discussed below, the fast spectroscopy is an essential feature for understanding the fast dynamics occurring in non-stationary operating points.

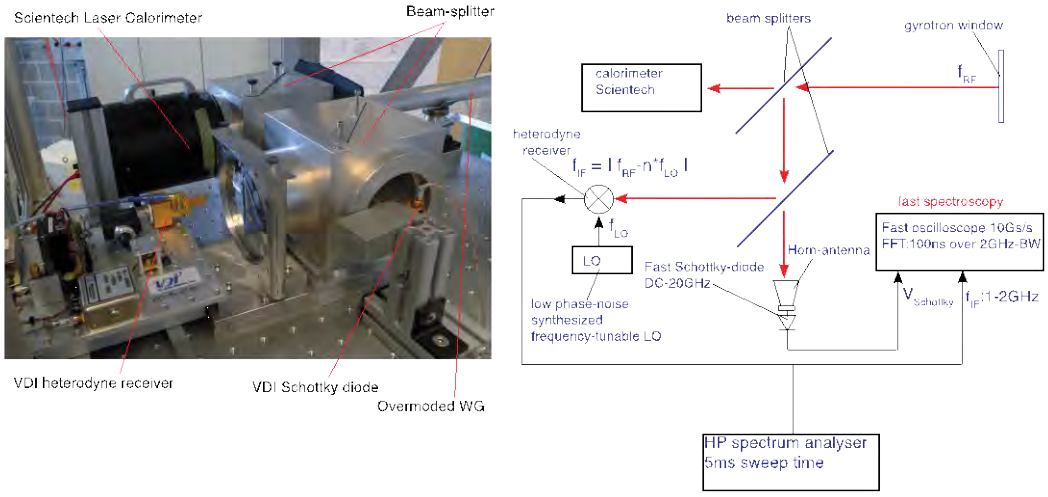


Fig. 4 On the left part is shown the layout of the rf-diagnostics used in this experiment with on the right part a corresponding schematic diagram. The fast Schottky diode signal (bandwidth dc to 20 *GHz*) and the intermediate frequency, $f_{IF}$, of the heterodyne receiver are acquired with a fast oscilloscope (2 *GHz* analogue bandwidth, 10 *Gpts/s*, 8 *bit* A/D converter). The $f_{IF}$ is also simultaneously acquired on a spectrum analyser with typically a 5 *ms* frequency sweep over a 2 *GHz* bandwidth.

## 3. Setup for DNP/NMR application and gyrotron results on stationary operating point

The experimental setup with the gyrotron mounted at the Nanostructured Materials Physics Laboratory (LPMN) of EPFL, where DNP/NMR experiments will be carried out is shown in Fig.5.

The stationary, single-frequency regime has been extensively characterized for the nominal operating transverse mode $TE_{7,2}$ radiating at 260 *GHz* and the two neighboring transverse modes, $TE_{4,3}$ and $TE_{2,4}$, radiating at 255 *GHz* and 265 *GHz*, respectively. In the nominal $TE_{7,2}$ mode operated in CW, with a very-high frequency and power stability (drift $\Delta f/f < 4$ *ppm*, $\Delta P_{RF}/P_{RF} < 1\%$), as shown in Fig.6 we have demonstrated a continuous frequency tunability, via the variation of the cavity magnetic field, over a 1.2 *GHz* frequency range with a rf power measured at the rf-window always exceeding 1.5 *W* and a maximum power of 150 *W*.

A very high-level of power and frequency stability has been reached using a PI controller on the cathode heating circuit which insures a long-term stability (CW) of the beam current, $I_b$, with fluctuations $\Delta I_b/I_b < 100$ *ppm*. In Fig.7 a long term frequency stability better than 1 *MHz* is demonstrated. The radiation line-width is essentially determined by the anode voltage fluctuations ($\delta V_a / V_a = 0.3\%$) and is as low as $\delta f = 3$ *MHz*.

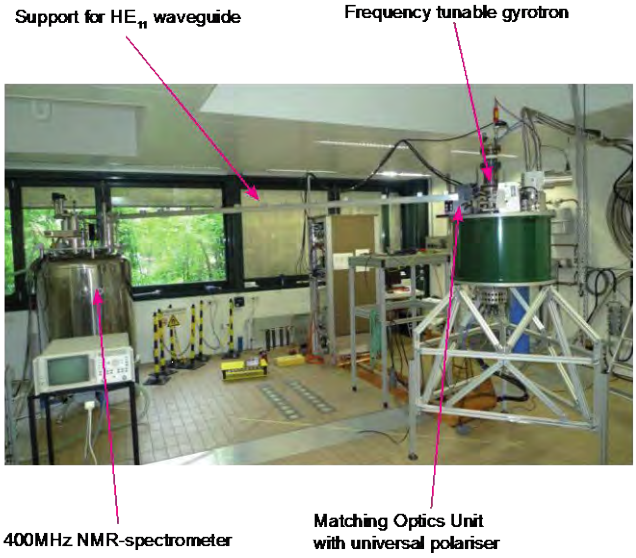


Fig.5 Layout of the DNP-NMR experiment with the gyrotron, the matching optics unit including a universal polarizer, the support of the $HE_{11}$ waveguide and the variable field 400 *MHz* NMR spectrometer. The 4 *m*-long $HE_{11}$ waveguide will be manufactured by the spin-off company of CRPP, Swissto12, using the stacked ring technique [19, 20].

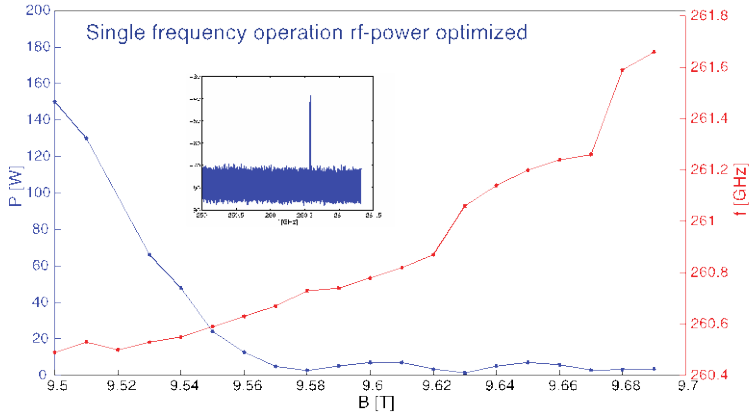


Fig. 6 Frequency tunability versus cavity magnetic field for the $TE_{7,2}$ mode (red curve). The blue curve shows the corresponding rf power. All points shown in this figure correspond to a stationary regime characterized by a single frequency (no side bands). At every magnetic field value, the rf-power has been optimized against the anode voltage, which is the control parameter for the pitch angle, with the constraint of maintaining a single-frequency oscillation.

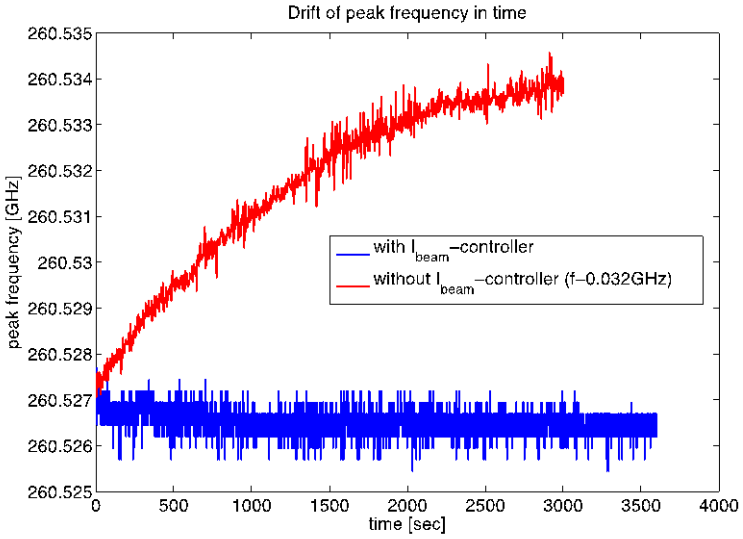


Fig. 7 Frequency-drift stabilization using a Proportional-Integral (PI) controller on the cathode heating. Red-curve without controller and blue-curve with PI controller. In both cases the gyrotron was operated in stationary operating points without side-band excitation.

In Fig.8 the pulsed regime via the fast control of the anode voltage on the triode MIG-gun is shown. rf pulse durations as short as 30 $\mu s$ and arbitrary duty cycle have been obtained. The shortest pulse-length is presently limited by the external stray-capacitance of the connecting circuits and might be further reduced.

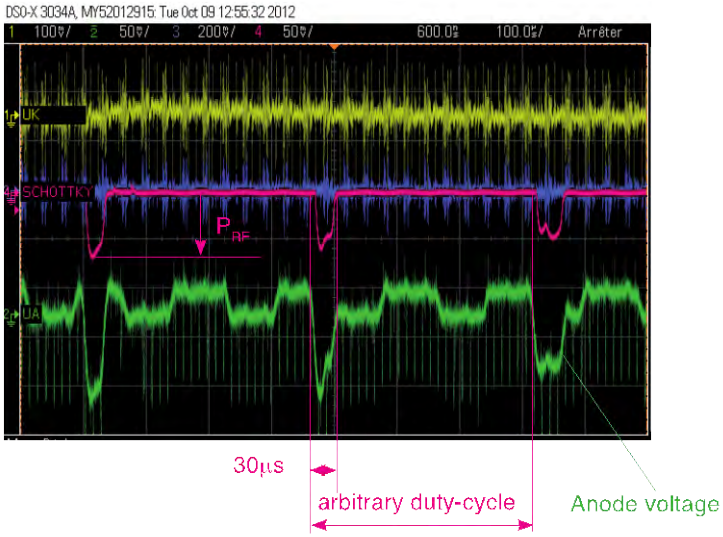


Fig. 8 Time traces of the pulsed regime ($TE_{7,2}$ at 260 *GHz*) via anode voltage modulation on the triode MIG-gun. In green is shown the AC part of the mod-Anode voltage. The periodic fluctuation on the anode voltage, with a period of approximately 160 $\mu s$, induces a pitch angle modulation, which is responsible of the line-width broadening of the side-bands as shown in Fig. 11 below. The red signal is measured with a fast Schottky diode (negative). The yellow and blue traces are the AC part of the accelerating voltage and the beam current respectively.

The output rf-beam characteristics have been determined using a phase retrieval method [21] and exhibit a very high Gaussian content. The phase retrieval technique has been applied to a set of transverse profiles taken with an infrared camera on a paper target. In the temperature range of the acquired transverse profile it has been verified that the target has a linear response versus rf power. The results of the rf beam characterization are summarized in Fig.9.

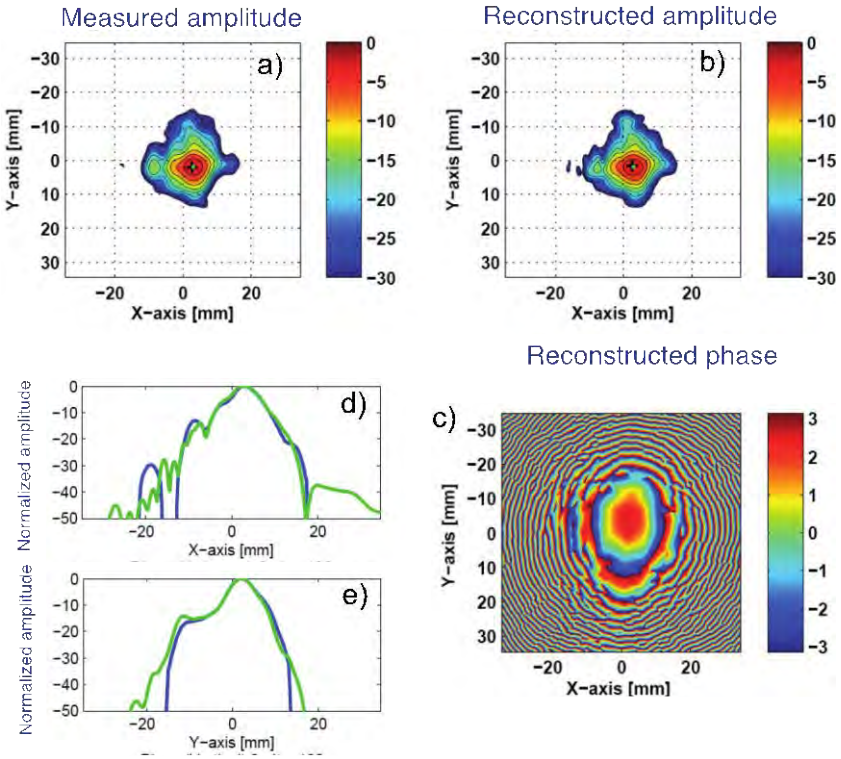


Fig. 9 Measured and reconstructed field pattern (z =70 *mm* after the gyrotron window) for the $TE_{7,2}$ mode. Sub-plot a) is the measured transverse profile with b) and c) the reconstructed amplitude and phase profiles [21]. Sub-plots d) and e) are transverse cuts on the x and y-axes of the measured (blue) and reconstructed (green) profiles.

## 4. New physics results on non-stationary operating points: chaotic regime and nanosecond pulse regime

In the following, as previously mentioned, we will concentrate on two specific operation points located in a region of the parameter space for which particular non-stationary regimes have been experimentally observed. These two points, A and B, are shown in Fig.10, on the left in the B-$I_b$ parameter space of Fig.1 and, on the right, using the uncoupled dispersion relation in the $\omega$-$k_{||}$ diagram. As discussed below, point A is characterized by periodic nanosecond pulses, of which the underlying physical mechanism is interpreted as a SQS phenomena. Point B is characterized by a frequency-doubling cascade eventually ending in a chaotic regime.

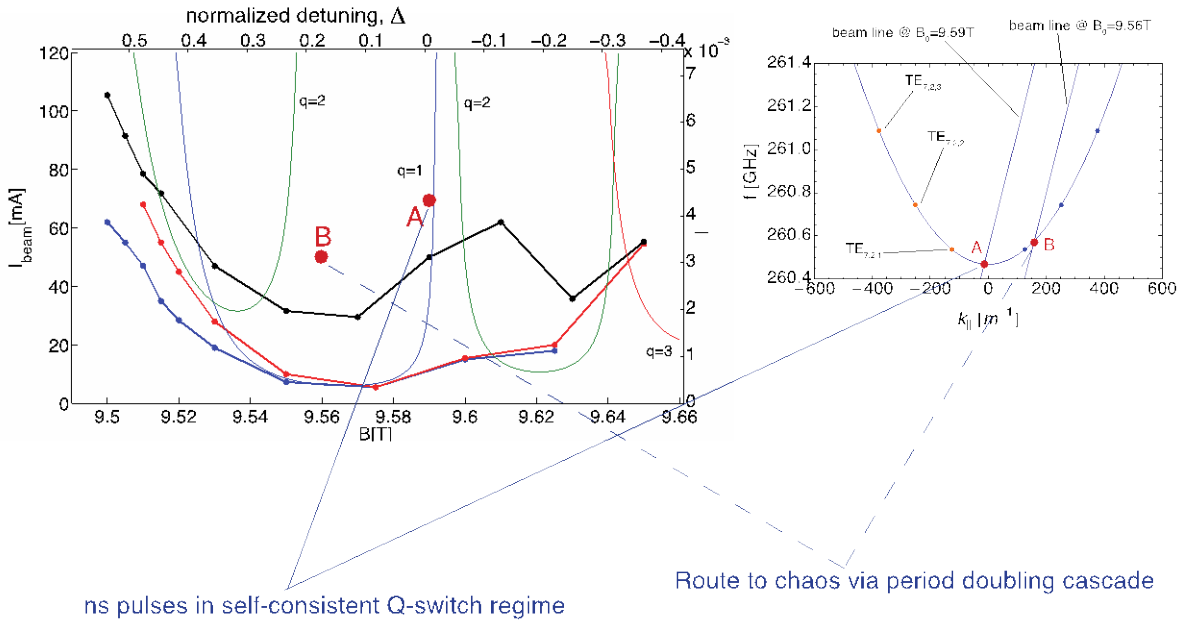


Fig. 10 Experimentally observed specific operating regimes are shown in the B-$I_b$ plane on the left (same parameter space as in Fig.1). On the right, uncoupled dispersion relation for the em-wave and the electron beam. Two specific operating points, A and B, are highlighted. The beam lines represent the Doppler-shifted beam dispersion relation for two cavity magnetic field values. The beam energy and pitch angle are 15.5 *keV* and 1.9, respectively. The filled dots on the wave dispersion relation ($TE_{7,2}$ mode) represent the discrete frequencies for a finite length cavity, $L_{eff}$ = 25 *mm*, with parallel wave-number $k_{||} = q\pi/L_{eff}$.

A first important comment to be made regards the relative values of the experimentally measured linear starting current, $I_{start}$, (red thick-line in Fig.10 left) and the starting current for non-stationary regimes, $I_{start\text{-}nonst}$ (black thick-line). The experimentally observed ratio, $I_{start\text{-}nonst}/I_{start}$ is between 1 and 10 and is also supported by the values obtained with the code TWANG. This ratio of $I_{start\text{-}nonst}/I_{start}$ is at least one order of magnitude lower than the one found by numerical simulations in [13]. As discussed in [11], this significant difference is probably associated to the over-simplified interaction space considered in [13].

Before discussing the operation on the two specific points A and B mentioned above, it is necessary to describe an interesting observed phenomenon related to the frequency sensitivity of the side-bands with respect to the anode-voltage fluctuations, ΔVa, inducing fluctuations on the electron beam pitch-angle. In Figure 11, are shown the time-trace of the applied anode voltage (subplot a), the corresponding time-resolved spectrogram (resolution, 300 *ns*) of the radiation frequency spectrum and, in subplot b), the frequency spectrum acquired with a slow-acquisition (5 *ms*) frequency analyser.

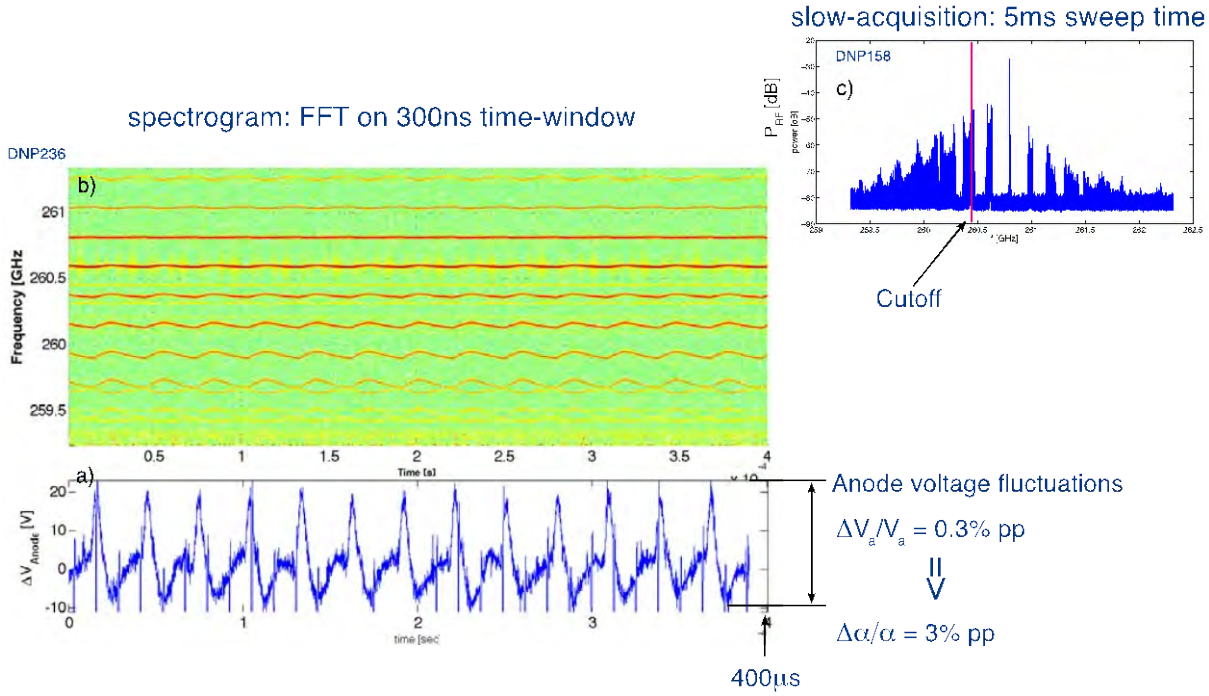


Fig. 11 Pitch-angle fluctuation sensitivity of side-bands. Subplot a) shows the time evolution of the anode voltage over a 400 $\mu s$ time window. On the same time window, subplot b) shows the spectrogram of the emitted radiation, calculated from the IF signal acquired with the fast-oscilloscope over a 300 *ns* time window. In subplot c) the shown spectrogram is acquired over a much longer time window, 5 *ms*, with the spectrum analyser. The vertical red line indicates the cutoff frequency in the constant radius cavity section, see Fig.3.

One observes a clear effect of the side-band frequency dependence on ΔVa. Moreover, the main frequency is nearly unaffected by ΔVa, whereas the frequency dependence increases for side-bands with increasing order. This broadening effect is clearly visible on subplots b) and c) where on c) it is evidenced by an artifact associated to the slow acquisition sweeping time of the spectrum analyser. The pitch-angle frequency sensitivity of the side-bands is consistent with numerical simulations with the code TWANG.

The experimentally observed « route to chaos via period doubling cascade » shown in Fig.12 has been possible by taking advantage of the pitch-angle frequency sensitivity of the side-bands discussed above. The experimentally observed period-doubling cascade is consistent with the theoretical prediction by Blokhina et al. [22] where this dynamics is observed in the vicinity of a zero normalized detuning. The quantitative comparison with [22] is however difficult since a simplified model has been considered and applied to simplified conditions for the system parameters (simplified cavity geometry, constant magnetic field, etc.). Strictly speaking the « route to chaos » shown in Fig.12 deviates from the so called « period doubling cascade » since, as shown, only the first branch of this cascade one observes « a period doubling » whereas for the following branches, « period tripling and quintupling » are observed. The explanation of this sequence is still under investigation, but one can mention that in other non-linear dynamical systems the « period tripling and quintupling » have been observed [23-25].

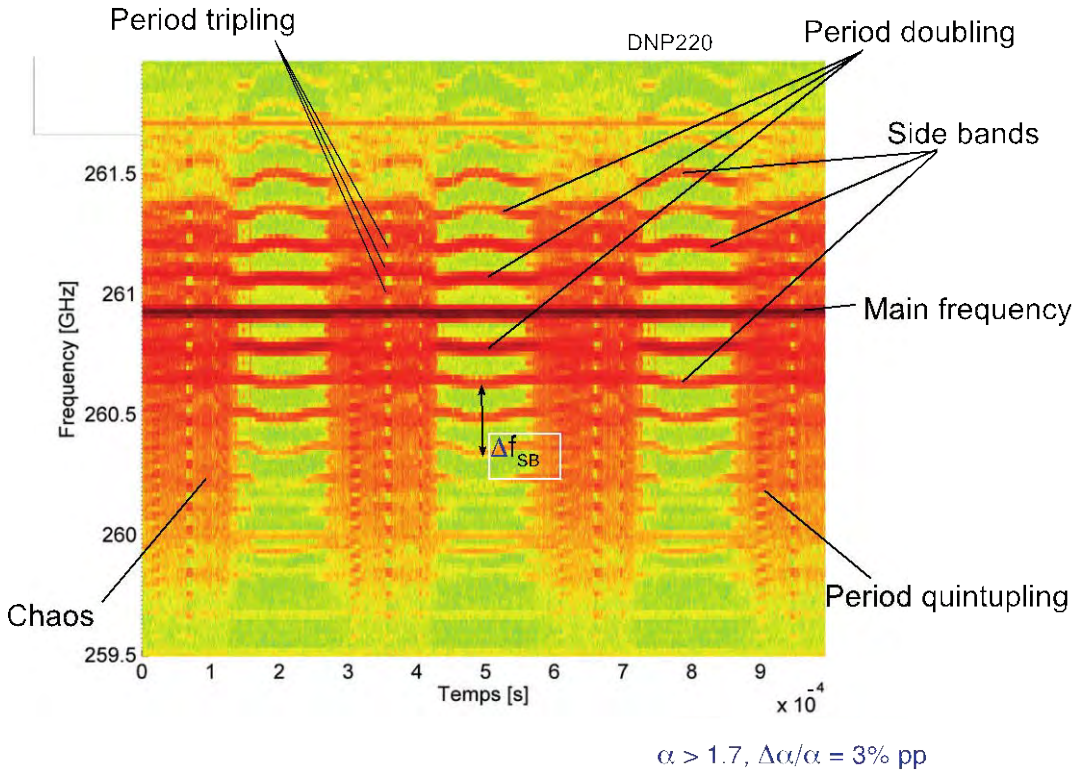


Fig. 12 Measured spectrogram of the gyrotron radiation spectra versus time for the "B" operating point shown in Fig.10. The frequency-doubling cascade is clearly visible. The time varying control parameter is the pitch-angle variation associated to periodic fluctuations (period = 30 *s*) of the anode voltage, $V_a$, with $\Delta V_{a\text{-}pp}/V_a \approx 0.3\text{-}0.5\%$ corresponding to a pitch angle fluctuation of $\Delta\alpha_{pp}/\alpha \approx 3\text{-}5\%$.

Another point of interest is the detailed synchronized frequency variation for spectral lines symmetric with respect to the main frequency. This suggests that all these spectral lines are phase-locked and we will come back to this point in the following section concerning the SQS regime. Finally, a detailed characterization of the wide variety of dynamical regimes for non-stationary operating points has been carried out both experimentally and in simulations [26].

The experimental evidence for the ns-pulse regime [12] is shown in Fig.13. As shown in the spectrogram (subplots b and c), what characterizes this regime is that the side-bands are exactly evenly spaced ($\Delta f = 240$ *MHz*) and the slight variation of their frequency separation is synchronous with the fluctuations of the anode voltage. This suggests that the side bands are phase-locked. Using a numerical homodyne detector we have determined that the relative phase between the side-bands varies typically less than $20^0$ over a 5 $\mu s$ time scale ; we therefore conclude that the side-bands are mutually phase-locked.

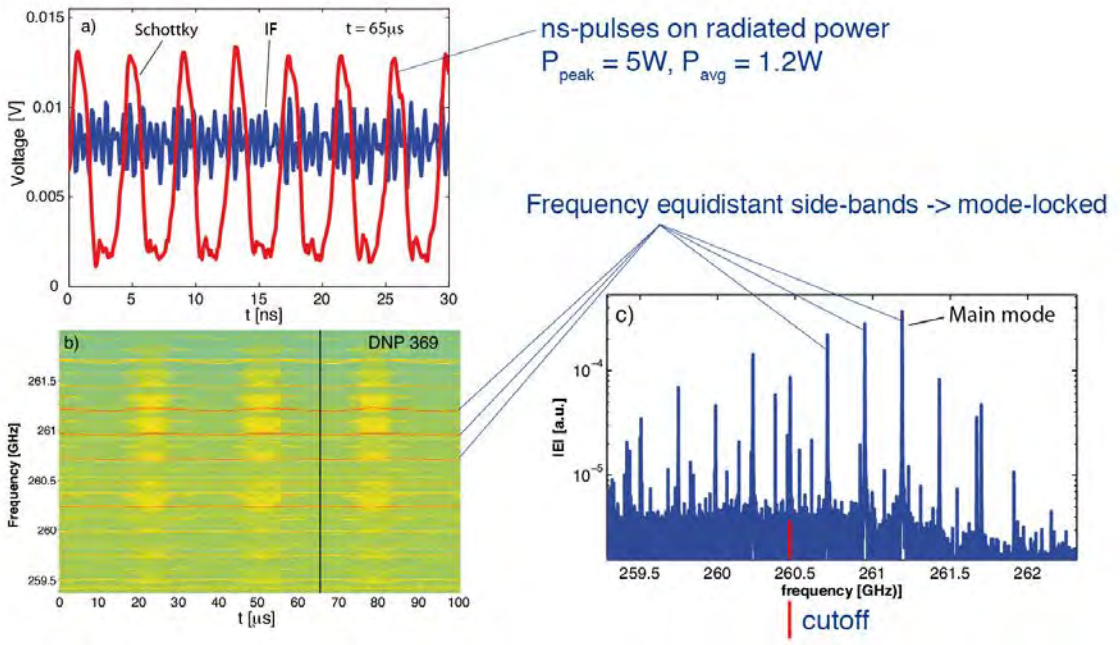


Fig. 13 Experimental measurement of nanosecond pulse regime. Subplot a): in red, fast Schottky diode (DC-20 *GHz* bandwidth) and, in blue, the IF of the heterodyne receiver. The FWHM of the rf pulses is 1ns with a 4.1 *ns* repetition rate. The time average rf power <Prf>=1.2 *W* with a peak power of 5 *W*. Subplot b) is a spectrogram with a time resolution of 100 *ns* and subplot c) is the measured spectrum taken at time = 65 $\mu s$ of the 100 $\mu s$ long aquired signal. One clearly observes that the side-bands are evenly spaced with a frequency separation of 240 *MHz*. The cutoff frequency in the constant cavity radius is indicated in subplot c) by the red line.

For the same system parameters as shown in Fig. 13, the relevant time-traces calculated with the TWANG code are shown in Fig. 14. A good agreement is found between the experimental and simulated data. From the calculated time traces it clearly appears that the pulsed regime is associated with a self-consistent variation of the loaded diffraction quality factor. It is important to remind that in this type of gyrotron (high-frequency, low-order transverse mode), the ohmic losses are as high as the diffraction losses[11]. The self-consistent modulation of the total quality factor is dominated by a very strong modulation of the diffraction losses. From subplot a) and b) of Fig.14 one observes that also the global quantities (i.e. integral quantities over the interaction space) are modulated with a characteristic period, $\tau = 4.1$ *ns*, equal to the inverse of the side-band separation. It has to be noticed that the electronic efficiency modulation exhibits nearly half a period with positive efficiency and the second-half with a negative efficiency. During the negative efficiency part, the electrons absorb energy from the electromagnetic wave. For the two local quantities (i.e. integral quantities over the output radiation surface), $P_{diff}$ and $Q_{diff}$ (see subplots c) and d) respectively), an even faster variation time scale is observed.

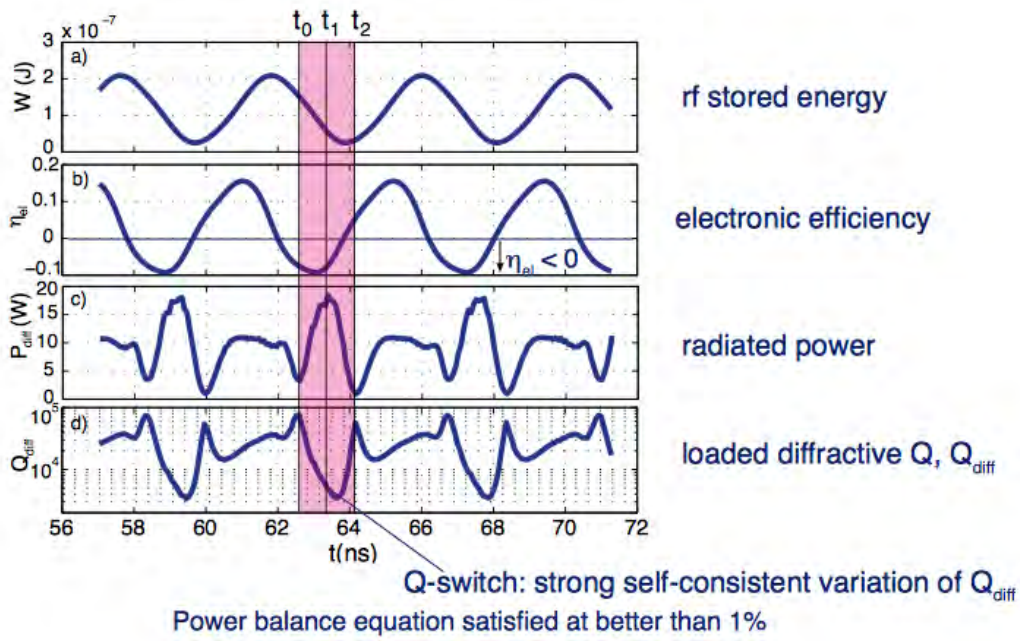


Fig. 14 Simulation results of the SQS regime calculated with TWANG. The system parameters are the same as for the experiment, and a cavity wall conductivity of $\sigma_{DC} = 1.4\ 10^9$ *S/m* has been considered. From top to bottom are the time traces of (a) cavity stored rf energy, (b) electronic efficiency, (c) radiated rf power measured at the cavity exit, (d) self-consistent diffraction quality factor.

## 5. Discussion and Conclusion

A detailed analysis of non-stationary regimes in gyrotron oscillators has been presented both with experimental results and theory. For the used theoretical model as well as for specific experimental aspects, it is important to emphasize on what are the characteristic time scales for the physics described in this paper. In Fig.15 these time scales are summarized on a logarithmic-scale time-axis and are labeled with regard to the points discussed below.

As commonly adopted, the gyro-averaged model (slow-time scale formulation of the wave-particle dynamics) together with the assumption that the electron time of flight in the interaction region, $\tau_b$, is significantly shorter than the time scale of the electromagnetic field amplitude variation, $\tau_{cav}$, allows to choose a time step for the numerical integration of the wave-equation, $\Delta t_{num}$, which is the order of magnitude higher than the fastest time scale, the cyclotron period. This is a very significant advantage in computing time with respect to full Particle-in-Cell (PIC) code which requires to have a numerical time step shorter than the cyclotron period. However, in presence of the observed fast-dynamics in non-stationary regimes the choice of, $\Delta t_{num}$, is limited by the characteristic time scale of this fast dynamics which can be associated to the wave transit time, $\tau_w << \tau_{cav}$. With this consideration one notices that, in presence of non-stationary regimes, the new time scale of the electromagnetic field amplitude variation is

$\tau_w$ which is comparable to $\tau_b$. Under these circumstances, despite the excellent qualitative and often quantitative agreement between experiment and theory, the model used in TWANG is arguable and a gyro-averaged Particle-in-Cell code would be more appropriate for properly handling all the relevant time scales.

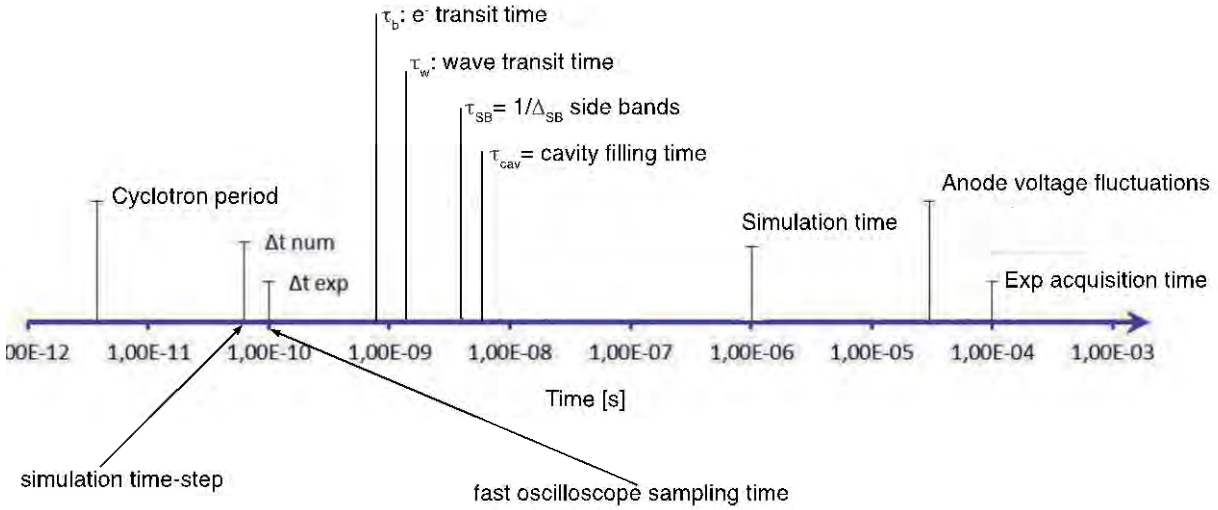


Fig. 15 Characteristic time scales associated to the non-stationary regimes described in this paper and the theoretical model used.

In summary a detailed analysis of the non-linear dynamics in gyrotron oscillators has been investigated both experimentally and theoretically. In a first part, a detailed characterization for DNP/NMR spectroscopy has been carried out for stationary operating points. In the second part, characterized by non-stationary regimes, the first experimental evidence of « route to chaos » via period doubling cascade has been demonstrated. A novel regime characterized by nanosecond pulses has been found and is interpreted as a self-consistent Q-switch mechanism in presence of phase-locked sidebands. This novel regime may open new applications for gyrotrons.

## Acknowledgments

S. Alberti would like to thank the organizers of the 4th SICAST conference for inviting him and giving the opportunity to present the material of this paper.

Work supported by Requip (206021-121303/1 and 206021_144983), Sinergia (CRSI20-122708/1), and (200020-120503/1) grants of the Swiss National Science Foundation, by the School of Basic Science/EPFL and by the EPFL. The authors would like to thank the precious work of all the EPFL staff involved in the experimental set-up. In particular, Ph. Cuanillon, G. Grandjean, M. Longchamp (IPMC) as well as D. Fasel, S. Allenspach, S. Couturier, and J. Dubray at CRPP.

## References

[1] Griffin, R. G. and Prisner, T. F. "High field dynamic nuclear polarization - the renaissance". *Phys. Chem. Chem. Phys.* 12, 5737 (2010).

[2] Vikram S. Bajaj, Melissa K. Hornstein, Kenneth E. Kreischer, et. al.. "250 GHz CW gyrotron oscillator for dynamic nuclear polarization in biological solid state NMR". *Journal of Magnetic Resonance.* 189, 251 (2007).

[3] Thorsten Maly, Galia T. Debelouchina, Vikram S. Bajaj, et. al.. "Dynamic nuclear polarization at high magnetic fields". *The Journal of Chemical Physics.* 128, No. 5, 052211 (2008).

[4] Stefano Alberti, Jean-Philippe Ansermet, Giuseppe Annino, et. al.. "THz-instrumentation development for gyrotron-DNP applications: from source to sample". *Proceedings of the Third International Symposium on Dynamic Nuclear Polarization,* 7-10 September 2011, Lausanne, Switzerland.

[5] Richard J. Temkin. "Terahertz Gyrotrons for Spectroscopy". *The 4th Shenzen International Conference on Advanced Science and Technology,* Nov. 3-9, 2013, Shenzen, China.

[6] Sakamoto Keishi, Kasugai Atsushi, Takahashi Koji, et. al.. "Achievement of robust high-efficiency 1MW oscillation in the hard-self-excitation region by a 170 GHz continuous-wave gyrotron". *Nat Phys,* 3, No. 6, 411 (2007).

[7] Keishi Sakamoto. "Development of high power gyrotron and related technology". *The 4th Shenzen International Conference on Advanced Science and Technology,* Nov. 3-9, 2013, Shenzen, China.

[8] Jelonnek J., Gantenbein G., Hesch K., et. al.. "From series production of gyrotrons for W7-X towards EU-1 MW gyrotrons for ITER". *Plasma Science (ICOPS), 2013 Abstracts IEEE International Conference on* (2013)

[9] M. Glyavin. "Gyrotrons development and application for plasma science and material processing". *The 4th Shenzen International Conference on Advanced Science and Technology,* Nov. 3-9, 2013, Shenzen, China.

[10] Alberti Stefano. "Magnetic confinement fusion: Plasma heating with millimetre waves". *Nat Phys,* 3, 6, 376 (2007).

[11] S. Alberti, J-Ph. Ansermet, K.A. Avramidis, et. al.. "Experimental study from linear to chaotic regimes on a terahertz-frequency gyrotron oscillator". *Phys. Plasmas*, 19, 123102 (2012).

[12] S. Alberti, F. Braunmueller, T.M. Tran, et. al.. "Nanosecond pulses in a THz gyrotron oscillator operating in a mode-locked self-consistent Q-switch regime". *Phys. Rev. Lett.,* 111, 205101 (2013).

[13] M.I. Airila and O. Dumbrajs. "Stochastic processes in gyrotrons". *Nucl. Fusion*, 43 1446 (2003).

[14] S. Alberti, T.M. Tran, K. Avraimidis, et. al.. "Gyrotron parasitic-effects studies using the time-dependent self-consistent monomode code TWANG". *Conference Digest, 36th International Conference on Infrared, Millemeter, and Terahertz Waves, Houston, Texas (USA) (2011).*

[15] N. S. Ginzburg, G. S Nusinovich, and N. A. Zavolsky. "Theory of non-stationary processes in gyrotrons with low Q resonators" *International Journal of Electronics,* 61, 6, 881 (1996).

[16] Chu, K. R.. "The electron cyclotron maser". *Rev. Mod. Phys.,* 76, 489 (2004).

[17] Chang T.H., Chen S.H., Barnett L.R., et. al.. "Characterization of Stationary and Nonstationary behavior in Gyrotron Oscillators". *Phys. Rev. Lett.,* 87, 064802-1 (2001).

[18] Nusinovich, G.S. "Review of the theory of mode interaction in gyrodevices". *IEEE Trans. on Plasma Science*, 27, 2, 313 (1999).

[19] E. de Rijk, A. Macor, J-Ph. Hogge, et. al.. "Note: Stacked rings for terahertz wave-guiding". *Rev. Sci. Instrum.*, 82, 066102 (2011).

[20] M. Thumm, D. Wagner, E. de Rijk, et. al.. "Multi-Frequency Notch Filters and Corrugated 500 to 750 GHz Waveguide Components Manufactured by Stacked Ring Technology". *The 4th Shenzen International Conference on Advanced Science and Technology,* Nov. 3-9, 2013, Shenzen, China.

[21] Jawla, S. and Hogge, J.-P. and Alberti, S. "Theoretical Investigation of Iterative Phase Retrieval Algorithm for Quasi-Optical Millimeter-Wave RF Beams". *IEEE Trans. on Plasma Science*, 37, 3, 403 (2009).

[22] Elena V. Blokhina, Sergey P. Kuznetsov, and Andrey G. Rozhnev. "High-Dimensional Chaos in a Gyrotron". *Electron Devices, IEEE Transactions on,* 54, 2, 188 (2007)

[23] Lamela H., Carpintero G., and Mancebo, F.J.. "Period tripling and chaos in the dynamic behavior of directly modulated diode lasers". *IEEE Journal of Quantum Electronics*, 34, 10, 1797 (1998)

[24] Wan Fung Ngai and Hai-Feng Liu. "Observation of period doubling, period tripling, and period quadrupling in a directly modulated 1.55 mu m InGaAsP distributed feedback laser diode". *Applied Physics Letters*, 62, 21, 2611 (1993).

[25] Braun Thomas, Lisboa Jorge A., Francke, Ricardo E., Gallas, et. al.. "Observation of deterministic chaos in electrical discharges in gases". *Phys. Rev. Lett.,* 59, 613 (1987).

[26] F. Braunmueller, J.Genoud, S. Alberti, et. al.. *in Proceedings of the 38th International Conference on Infrared, Millimeter and Terahertz Waves*, Mainz, Germany, 2013, paper Mo1-5 (to be published).